Materials Advances

ROYAL SOCIETY OF CHEMISTRY

PAPER

View Article Online
View Journal | View Issue

Check for updates

Cite this: *Mater. Adv.*, 2023, 4, 3270

Halogen functionalized D–A–D-type unsymmetrical squaraine dyes for dye-sensitized solar cells†

Indrajeet S. Nawghare,[ac] Ambarish Kumar Singh,[ac] Ashakiran Maibam,[ac] Shivdeep Suresh Deshmukh,[ac] Sailaja Krishnamurty,*[ac] Kothandam Krishnamoorthy *[bc] and Jayaraj Nithyanandhan *[ac]

Received 2nd June 2023,
Accepted 26th June 2023

DOI: 10.1039/d3ma00277b

rsc.li/materials-advances

The development of sensitizers with the D–A–D architecture with an indoline donor and squaryl acceptor is attractive towards achieving the high-efficiency dye-sensitized solar cells (DSSCs) due to an intense absorption ($\varepsilon > 10^5$ M^{-1} cm^{-1}) in the far-red region and dye aggregation behaviour on the mesoporous TiO_2 surface, which broadens the light harvesting properties. To further enhance the photovoltaic parameters, features that help to enhance the charge injection and dye-regeneration processes must be built into the sensitizers, and the charge recombination must be diminished. Here, a series of squaraine dyes (**ISQ**) in which an alkyl-group-wrapped indoline donor functionalized with a halogen atom, which is separated from another indoline donor that contains an anchoring group, have been designed and synthesized. Photophysical, electrochemical and photovoltaic characterizations have been carried out to understand the effect of the halogen atom on their electronic, photo-excited and DSSC device properties. Photophysical characterization revealed the singlet nature of the photo-excited state despite the presence of a heavy atom such as iodine, bromine and chlorine in the **ISQ** dyes. The singlet excited state lifetime and the fluorescence quantum yield for the **ISQ** dyes were almost equal to or slightly higher than those of the **ISQ-H** dye. The molecular electrostatic potential obtained from DFT studies indicated the presence of a σ-hole in the halogen-functionalized **ISQ** dyes, which assists in the dye regeneration process through halogen bonding. DSSC devices were fabricated with iodolyte electrolytes in high (Z-150) and low (Z-50) redox concentrations in order to determine the importance and effect of halogen functionalization in squaraine dyes on the DSSC performance. Different photovoltaic performances were observed for the **ISQ** dyes when the devices were fabricated with the Z-50 and Z-150 iodolyte electrolytes. A maximum DSSC efficiency of 6.48% was achieved using **SQS4** dye in Z-50 without CDCA, and an efficiency of 7.80% was achieved using **ISQ-I** dye in Z-150 with CDCA.

1. Introduction

In the context of third-generation photovoltaic devices, dye-sensitized solar cells (DSSCs) in particular offer avenues to modulate the charge-transfer dynamics across various interfaces *via* the design of the photoanode, dye, electrolyte and cathode materials for enhanced device performance.[1–6] Synergistic integration of interfacial properties is required to achieve the required charge injection, dye-regeneration and transport processes while minimizing charge-recombination processes.[3,6–9] Metal-free organic dyes with different architectures have been utilized to harvest visible and NIR photons for photocurrent generation, in addition to sensitizers based on the ruthenium–polypyridine and zinc–porphyrin complexes.[10] Indeed, the cheap precursors, easy synthesis, and modular photophysical and electrochemical properties of metal-free organic dyes make them very attractive compared to metal-containing dyes.[11–15] The aggregation of dyes on nano-crystalline TiO_2 is a facile process due to the presence of periodical 5-coordinated Ti

[a] *Physical and Materials Chemistry Division, CSIR-National Chemical Laboratory, CSIR-Network of Institutes for Solar Energy, Dr Homi Bhabha Road, Pune, 411008, India. E-mail: j.nithyanandhan@ncl.res.in, k.krishnamoorthy@ncl.res.in, k.sailaja@ncl.res.in*
[b] *Polymer Science and Engineering Division, CSIR-National Chemical Laboratory, and CSIR-Network of Institutes for Solar Energy, Dr Homi Bhabha Road, Pune, 411008, India*
[c] *Academy of Scientific and Innovative Research (AcSIR), Ghaziabad, 201002, India*

† Electronic supplementary information (ESI) available: General methods, DSSC device fabrication, ^{1}H- and ^{13}C-NMR, IR, DFT, EIS and dye-desorption study of **ISQ** dyes are provided in the ESI. See DOI: https://doi.org/10.1039/d3ma00277b

centres (in which a dye forms a covalent bond with the anchoring group) in the anatase 101 facet, which has been considered to be a detrimental factor for DSSC device performance.[16–18] However, one of the design principles to control the aggregation of the dyes on the TiO_2 surface is tailoring the hydrophobic alkyl groups in the sensitizer, which also helps in passivating/shielding the surface to minimize the charge recombination of electrons in TiO_2 with oxidized electrolyte species.[19–22] It is known that the dye regeneration kinetics affect the photovoltaic parameters such as V_{OC} and J_{SC} in DSSC performance.[8,23] Hence, integrating the features to enhance the dye regeneration process in the dye is a very attractive and important aspect, in addition to the built-in electronic and steric factors of the sensitizers.[24–27] Furthermore, in order to enhance the dye regeneration efficiency, the inclusion of triphenylamine-based additives in the electrolyte[28] and functionalization of the dye with bulky 3D-triarylamine donors have been reported.[29]

Halogen bonding has been utilised in chemistry as well as in chemical biology due to its highly directional intermolecular interactions.[30–32] In this regard, polarizable atoms such as the –Br or –I atom have been integrated with D–π–A based sensitizers in conjunction with an I^-/I_3^- based electrolyte, as the non-covalent interaction between a halogen atom of the oxidised dye and the iodide ions in the electrolyte facilitate dye regeneration.[26,27] Additionally, a pyridyl-donor-based D–π–A dye on TiO_2 showed enhanced regeneration kinetics with a cobalt electrolyte for improved device performance by improving the interaction between the dye and the cobalt electrolyte through the pyridyl unit in the dye.[33–35] Hence, integration of a functional moiety that helps to promote the dye-regeneration process by either halogen-bonding or halogen-bonding (σ-hole in the halogen-atom-containing dyes) with a Lewis base are very important to enhance the DSSC device J_{SC} and efficiency.[25,34] As there are only a few chromophores that harvest photons in the far-red and NIR regions of the solar spectrum, such as porphyrin- and phthalocyanine-based dyes, it is important to develop metal-free organic dyes for dye-sensitized solar cells. Squaraine dyes from polymethine chromophores absorb in the far-red region of the spectrum with a high extinction coefficient.[36,37] An *N*-alkylated unsymmetrical squaraine dye exhibited a DSSC device efficiency of 4.5% (V_{OC} = 603 mV and J_{SC} = 10.5 mA cm^{-2}).[38] Extending the π-conjugation "outside the polymethine framework" with a naphthalene donor unit,[39] dithienothiophene[40] and thiophene[41] π-spacers increased the DSSC device performance to 5.4% (V_{OC} = 667 mV and J_{SC} = 11.3 mA cm^{-2}), 6.0% (V_{OC} = 644 mV and J_{SC} = 13.1 mA cm^{-2}) and 6.74% (V_{OC} = 642 mV and J_{SC} = 14.8 mA cm^{-2}), respectively. Additionally, the alkyl-group-wrapped squaraine dye **SQS4** showed a device efficiency of 7.1% (V_{OC} = 715 mV and J_{SC} = 13.05 mA cm^{-2}).[21] Wrapping the squaraine dye with alkyl groups helps to control the aggregation of dyes as well as to passivate the TiO_2 surface efficiently to enhance the J_{SC} and V_{OC} of the DSSC devices, respectively. Furthermore, to enhance the dye regeneration process with the D–A–D type squaraine dyes, a halogen-bonding interaction between the oxidized sensitizer and iodine ion in the electrolyte is envisaged. Hence, functionalization of the squaraine dyes with a halogen atom is designed in the present investigation. As it is reported in the literature that functionalizing the organic chromophores enhances the intersystem-crossing process,[43,44] the excited state properties of halogen-functionalized squaraine dyes have been studied in detail.

Systematic photophysical, electrochemical, theoretical, and photovoltaic characterizations have been carried out to investigate the effect of the squaraine dye with halogen functionality on the photovoltaic performance. The structures of the halogen functionalized D–A–D-based **ISQ** dyes are provided in Fig. 1.

2. Experimental section

Compounds **2**, **4c**, and **5** have been reported in the literature.[21,42] Hydrazine derivatives **1a–d** and 1-iodododecane are commercially available.

2.1. General procedure for the synthesis of 3-decyl-3-dodecyl-5-halo-2-methyl-3*H*-indoles, (3a–d)

Halogen-substituted phenylhydrazine hydrochloride (**1**) and 3-decylpentadecan-2-one (**2**) (1.3 equiv.) were dissolved in 10 mL of AcOH in a 50 mL round-bottom flask. The reaction mixture was refluxed under a nitrogen atmosphere for 24 h. The reaction mixture was cooled, the solvent was removed under reduced pressure, and the product was purified *via* column chromatography (100–200 mesh SiO_2) using EtOAc and petroleum ether as the eluents.[42]

2.1.1. 3-Decyl-3-dodecyl-5-fluoro-2-methyl-3*H*-indole (3a). Starting materials **1a** (0.5 g, 3.07 mmol) and 3-decylpentadecan-2-one (1.46 g, 3.99 mmol, 1.3 equiv.), reaction time 24 h, column chromatography (SiO_2, 100–200 mesh, 5% EtOAc and 95% pet. ether). Yield: 0.77 g, 54%. ^{1}H NMR ($CDCl_3$, 400 MHz): δ 7.43 (m, 1H), 6.97 (m, 1H), 6.89 (m, 1H), 2.19 (s, 3H), 1.86–1.68 (m, 4H), 1.29–1.10 (m, 30 H), 0.89–0.84 (m, 8H), 0.73–0.67 (m, 2H), 0.68–0.54 (m, 2H); ^{13}C NMR ($CDCl_3$, 100 MHz): δ 186.4, 161.2 (d, J = 244 Hz), 151.0, 144.4 (d, J = 9 Hz), 120.1 (d, J = 9 Hz), 114.0 (d, J = 24 Hz) 109.3 (d, J = 25 Hz), 63.2, 45.70, 36.9, 32.4, 31.8, 29.5, 29.7, 29.5, 29.2, 27.5, 23.5, 22.6, 15.9, 14.1. MALDI-TOF (m/z): $[M]^+$ 457.288.

2.1.2. 3-Decyl-3-dodecyl-5-chloro-2-methyl-3*H*-indole (3b). Starting materials (4-chlorophenyl)hydrazine hydrochloride (0.5 g, 2.79 mmol) and 3-decylpentadecan-2-one (1.33 g, 3.63 mmol, 1.3 equiv.), reaction time 24 h, column chromatography (SiO_2, 100–200 mesh, 2% EtOAc and 98% pet. ether). Yield: 0.60 g, 45%. ^{1}H NMR ($CDCl_3$, 200 MHz): δ 7.42 (d, J = 8 Hz, 1H), 7.25 (dd, J = 8 Hz, 4 Hz, 1H), 7.15 (d, J = 4 Hz, 1H), 2.20 (s, 3H), 1.87–1.80 (m, 2H), 1.75–1.66 (m, 2H), 1.24–1.10 (m, 30 H), 0.89–0.84 (m, 8 H), 0.71–0.65 (m, 2H), 0.60–0.53 (m, 2H); ^{13}C NMR ($CDCl_3$ 100 MHz): δ 187.2, 154.0, 144.7, 130.6, 124.1, 120.9, 118.9, 63.2, 45.7, 37.02, 32.4, 31.9, 29.8, 29.6, 29.5, 29.2, 27.5, 23.6, 22.7, 16.08, 14.2. MALDI-TOF (m/z): $[M]^+$ 473.286.

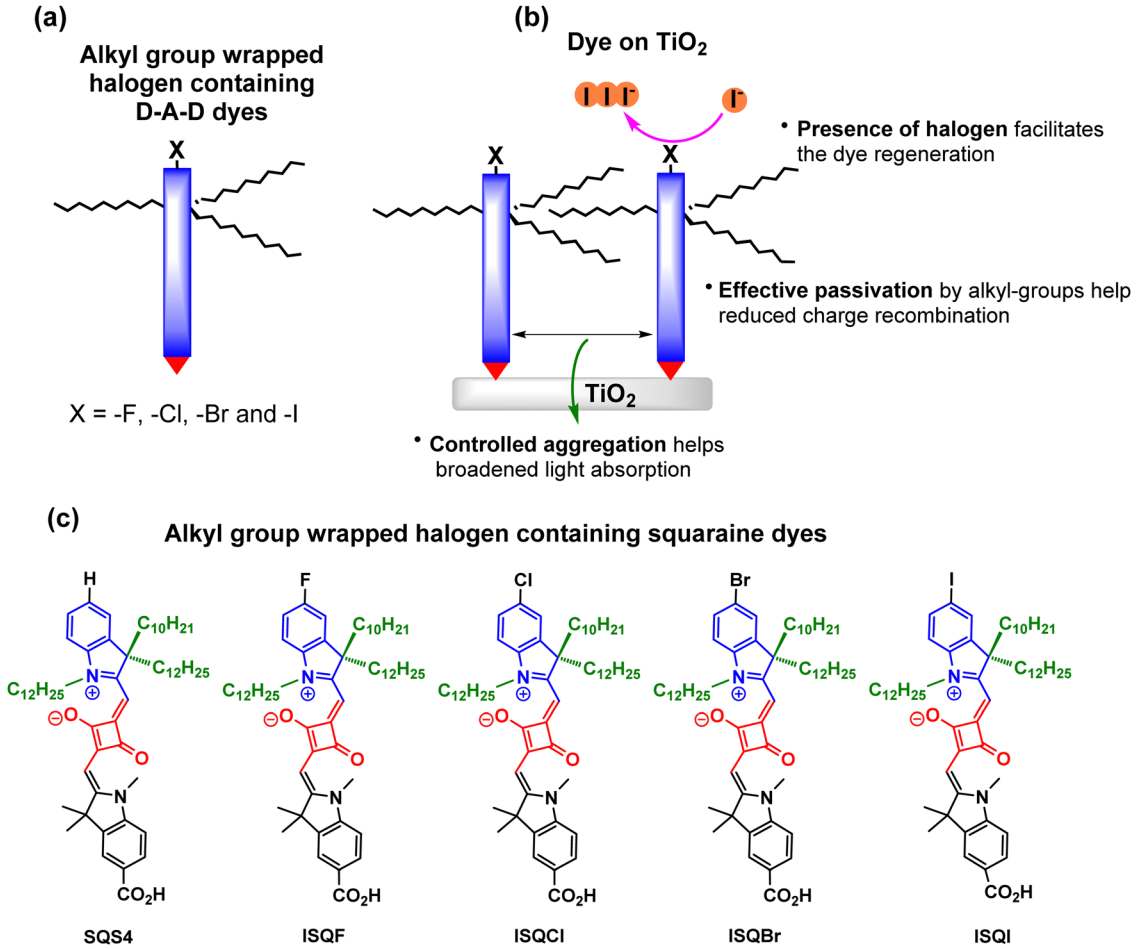

Fig. 1 (a) Schematic representation of the alkyl-group-wrapped halogen-containing dye and (b) the self-assembly of dyes on the TiO_2 surface. (c) Structures of the targeted squaraine dyes.

2.1.3. 5-Bromo-3-decyl-3-dodecyl-2-methyl-3*H*-indole (3c). Starting materials (4-bromophenyl)hydrazine hydrochloride (0.5 g, 2.23 mmol) and 3-decylpentadecan-2-one (1.06 g, 2.90 mmol, 1.3 equiv.), reaction time 24 h, column chromatography (SiO_2, 100–200 mesh, 1% ethyl acetate and 99% pet. ether). Yield: 0.55 g, 47%. ^{1}H NMR ($CDCl_3$, 500 MHz): δ 7.43–7.25 (m, 3H), 2.19 (s, 3H), 1.86–1.81 (m, 2H), 1.72–1.65 (m, 2H) 1.24–1.11 (m, 30 H), 0.85–0.88 (m, 8H), 0.68 (m, 2H), 0.56 (m, 2H); ^{13}C NMR ($CDCl_3$ 100 MHz): δ 187.1, 154.8, 145.0, 136.5, 130.7. 121.4, 63.2, 45.6, 36.9, 32.3, 31.8, 29.7, 29.6, 29.4, 29.1, 27.4, 23.5, 22.6, 16.0, 14.1. MALDI-TOF (m/z): $[M + H]^+$ 518.288.

2.1.4. 3-Decyl-3-dodecyl-5-iodo-2-methyl-3*H*-indole (3d). Starting materials 4-iodophenylhydrazine hydrochloride (0.34 g, 1.25 mmol) and 3-decylpentadecan-2-one (0.59 g, 1.63 mmol, 1.3 equiv.), reaction time 24 h, column chromatography (SiO_2, 100–200 mesh, 2% EtOAc and 98% pet. ether). Yield: 0.29 g, 40%. ^{1}H NMR ($CDCl_3$, 400 MHz): δ 7.63 (dd J = 8 Hz, 4 Hz, 1H), 7.50 (d, J = 4 Hz, 1H), 7.28 (d, J = 8 Hz, 1H), 2.19 (s, 3H), 1.78–1.86 (m, 2H), 1.66–1.74 (m, 2H), 1.10–1.25 (m, 30H), 0.85–0.89 (m, 8H), 0.64–0.71 (m, 2H), 0.51–0.59 (m, 2H); ^{13}C NMR ($CDCl_3$ 100 MHz): δ 195.3, 161.0 (d, J = 228 Hz), 141.3 (d, J = 9 Hz), 138.2, 117.7 (d, J = 10.6 Hz), 117.1 (d, J = 25 Hz), 111.4 (d, J = 25 Hz), 90.1, 63.2, 45.1, 36.9, 31.9, 29.8, 29.6, 29.5, 29.2, 23.5, 22.7, 16.1, 14.2. MALDI-TOF (m/z): $[M + H]^+$ 566.302.

2.2. General procedure for the synthesis of halogen-substituted iodolium salts (4a–d)

1-Iodododecane (1.3 equiv.) and corresponding the 3-decyl-3-dodecyl-5-halo-2-methyl-3*H*-indole (**3a–d**) (1 equiv.) were dissolved in CH_3CN (10 mL) in a 50 mL round-bottom flask and refluxed under a nitrogen atmosphere. The reaction mixture was cooled, and the solvent was evaporated under reduced pressure. The reaction mixture was washed with *n*-pentane (5 × 2 mL) to obtain the required compound as a brown-red viscous liquid.[42]

2.2.1. 3-Decyl-1,3-didodecyl-5-fluoro-2-methyl-3*H*-indol-1-ium (4a). Starting materials **3a** (0.63 g, 1.38 mmol) and 1-iodododecane (0.53 g, 1.80 mmol), reaction time 48 h. Yield: 0.72 g, 68%. ^{1}H NMR ($CDCl_3$, 400 MHz): δ 7.88 (m, 1H), 7.29 (m, 1H), 7.15 (m, 1H), 4.85 (t, J = 7.26 Hz, 2H), 3.12 (s, 3H), 2.06–2.04 (m, 2H), 1.71–1.77 (m, 2H), 1.07–1.19 (m, 54H), 0.81–0.78 (m, 9H), 0.59–0.61 (m, 2H); ^{13}C NMR ($CDCl_3$, 100 MHz): δ 195.4, 161.0 (d, J = 228 Hz), 141.3 (d, J = 9 Hz), 138.2, 120.0, 117.7 (d, J = 10 Hz), 117.1 (d, J = 25 Hz),

111.4 (d, J = 25 Hz), 63.8, 50.9, 37.2, 33.5, 31.8, 30.4, 29.5, 29.3, 28.5, 26.9, 24.08, 22.6, 17.5, 15.9, 14.1.

2.2.2. 5-Chloro-3-decyl-1,3-didodecyl-2-methyl-3*H*-indol-1-ium (4b). Starting materials **3b** (0.42 g, 0.56 mmol) and 1-iodododecane (0.22 g, 0.734 mmol), reaction time 48 h. Yield: 0.185 g, 71%. ^{1}H NMR ($CDCl_3$, 400 MHz): δ 7.83 (d, J = 8 Hz, 1H), 7.63 (dd, J = 8 Hz, 4 Hz, 1H), 7.47 (d, J = 4 Hz, 1H), 4.92 (t, J = 7.26 Hz, 2H), 3.19 (s, 3H), 1.80–1.84 (m, 4H), 1.10–1.26 (m, 52H), 0.84–0.88 (m, 9H), 0.66–0.70 (m, 2H), 0.55–0.58 (m, 2H); ^{13}C NMR $CDCl_3$ 100 MHz): δ 195.9, 140.8, 140.6, 136.8, 130.2, 124.0, 116.9, 63.9, 63.2, 51.1, 45.6, 37.0, 33.6, 31.9. 29.7, 29.5, 29.3, 23.5, 22.7, 17.6, 16.1, 14.2.

2.2.3. 5-Bromo-3-decyl-1,3-didodecyl-2-methyl-3*H*-indol-1-ium (4c). Starting materials **3c** (0.56 g, 1.08 mmol) and 1-iodododecane (0.41 g, 1.40 mmol), reaction time 48 h. Yield: 0.62 g, 70%. ^{1}H NMR ($CDCl_3$, 400 MHz): δ 7.81 (m, 1H), 7.66–7.64 (m, 2H), 4.81 (t, J = 7.26 Hz, 2H), 3.05 (s, 3H), 2.12 (m, 4H), 1.91 (m, 2H), 1.17–1.25 (m, 52H), 1.85–0.88 (m, 9H), 0.69–0.72 (m, 2H); ^{13}C NMR ($CDCl_3$ 100 MHz): δ 195.8, 141.3, 140.9, 133.0, 126.9, 124.6, 117.2, 63.8, 51.0, 45.3, 37.2, 33.5, 31.9, 30.5, 29.6, 29.4, 29.3, 28.5, 26.9, 24.1, 22.6, 14.1.

2.2.4. 3-Decyl-1,3-didodecyl-5-iodo-2-methyl-3*H*-indol-1-ium (4d). Starting materials **3d** (0.32 g, 0.56 mmol) and 1-iodododecane (0.21 g, 0.73 mmol), reaction time 48 h. Yield: 0.315 g, 75%. ^{1}H NMR ($CDCl_3$, 400 MHz): δ 8.0–7.98 (m, 2H), 7.84 (d, J = 4 Hz. 1H), 4.84 (t, J = 7.26, 2H), 3.18 (s, 3H), 1.78–1.83 (m, 4H) 1.10–1.26 (m, 57H), 0.85–1.13 (m, 4H), 0.67–0.72 (m, 2H), 0.53–0.65 (m, 2H); ^{13}C NMR ($CDCl_3$ 100 MHz): δ 195.5, 141.0, 138.9, 132.7, 128.9, 125.4, 96.2, 63.8, 63.2, 37.3, 36.9, 33.5, 31.9, 29.6, 29.4, 29.3, 28.5, 24.1, 22.7, 22.6, 16.02, 14.1.

2.3. Synthesis of unsymmetrical ISQ dyes (ISQF, ISQCl, ISQBr and ISQI)

Compound **4a–d** (1 equiv.) and **5** (1 equiv.) were dissolved in *n*-butanol and anhydrous PhMe (1 : 1, 10 mL of each) in a 50 mL round-bottom flask equipped with a Dean–Stark apparatus and refluxed under an inert atmosphere for 24 h. The reaction mixture was cooled, the solvents were removed under reduced pressure and the products were purified using column chromatography (100–200 mesh SiO_2, CH_2Cl_2:MeOH) to obtained the required dyes.[21]

2.3.1. (*E*)-4-((5-Carboxy-1,3,3-trimethyl-3*H*-indol-1-ium-2-yl)-methylene)-2-(((*Z*)-3-decyl-1,3-didodecyl-5-fluoroindolin-2-ylidene)-methyl)-3-oxocyclobut-1-en-1-olate (ISQF). Starting materials **4a** (0.49 g, 0.66 mmol) and **5** (0.20 g, 0.66 mmol), reaction time 24 h, column chromatography (SiO_2, 100–200 mesh, from 1.5% MeOH and 98.5% CH_2Cl_2). Yield: 0.20 g, 32%. ^{1}H NMR ($CDCl_3$, 400 MHz): δ 8.12 (d, J = 8 Hz, 1H), 8.05 (s, 1H), 7.05 (d, J = 8 Hz, 2H), 6.98 (d, J = 8 Hz, 2H), 6.14 (s, 1H), 5.98 (s, 1H), 4.04 (b, 2H), 3.52 (s, 3H), 3.05 (b, 2H), 1.99–1.95 (m, 2H), 1.84 (s, 8H), 1.43–1.38 (m, 2H), 1.25–1.06 (m, 52H), 0.88–0.76 (m, 8H), 0.76 (b, 2H), 0.47 (b, 2H); ^{13}C NMR ($CDCl_3$, 100.61 MHz): δ 181.7, 176.5, 170.4, 168.8, 161.8, 159.4, 147.4, 141.8, 139.1, 131.2, 124.4, 124.0, 123.5, 114.6 (d, J = 24 Hz), 110.4, 110.3 (d, J = 25 Hz), 108.1, 88.6, 88.1, 59.6, 48.3, 44.4, 40.3, 35.0, 31.9, 29.6, 29.6, 29.5, 29.4, 29.3, 27.3, 24.1, 22.7, 22.7, 14.1; IR (cm^{-1}): 2956, 2920, 2851, 1698, 1597, 1565, 1503, 1495, 1468, 1442, 1355, 1261, 1206, 1176, 1082, 1052, 935, 844, 812, 793, 772, 737, 711, 689; MALDI-TOF (m/z): $[M]^+$ 921.799.

2.3.2. (*E*)-4-((5-Carboxy-1,3,3-trimethyl-3*H*-indol-1-ium-2-yl)-methylene)-2-(((*Z*)-5-chloro-3-decyl-1,3-didodecylindolin-2-ylidene)-methyl)-3-oxocyclobut-1-en-1-olate (ISQCl). Starting materials **4b** (0.4 g, 0.62 mmol) and **5** (0.19 g, 0.62 mmol), reaction time 24 h, column chromatography (SiO_2, 100–200 mesh, from 1% MeOH and 99% CH_2Cl_2). Yield: 0.22 g, 36%. ^{1}H NMR ($CDCl_3$, 400 MHz): δ 8.12 (d, J = 8 Hz, 1H), 8.05 (s, 1H), 7.32 (d, J = 8 Hz, 2H), 7.0 (d, J = 8 Hz, 1H), 6.92 (d, J = 8 Hz, 1H), 6.15 (s, 1H), 6.01 (s, 1H), 4.02 (b, 2H), 3.54 (s, 3H), 3.04 (b, 2H), 1.99–1.96 (m, 2H), 1.84 (s, 8H), 1.43–1.38 (m, 2H), 1.26–1.06 (m, 53H), 0.89–0.81 (m, 8H), 0.74 (b, 2H), 0.48 (b, 2H); ^{13}C NMR ($CDCl_3$, 100.61 MHz): δ 182.4, 178.1, 170.4, 170.1, 169.2, 147.4, 142.6, 141.9, 131.3, 130.1, 127.1, 124.1, 122.8, 110.4, 108.2, 88.3, 59.3, 48.4, 40.1, 31.9, 29.7, 29.6, 29.6, 29.5, 29.4, 29.3, 27.3, 24.1, 22.7, 14.1; IR (cm^{-1}): 2955, 2920, 2852, 1699, 1597, 1566, 1504, 1485, 1466, 1425, 1350, 1261, 1179, 1084, 1055, 934, 842, 801, 772, 739, 688, 666; MALDI-TOF (m/z): $[M]^+$ 937.726 $[M + H]^+$ and 939.53 $[M + H + 2]^+$.

2.3.3. (*E*)-2-(((*Z*)-5-Bromo-3-decyl-1,3-didodecylindolin-2-yl-idene)methyl)-4-((5-carboxy-1,3,3-trimethyl-3*H*-indol-1-ium-2-yl)-methylene)-3-oxocyclobut-1-en-1-olate (ISQBr). Starting materials **4c** (0.77 g, 0.95 mmol) and **5** (0.3 g, 0.95 mmol), reaction time 24 h, column chromatography (SiO_2, 100–200 mesh, from 1% MeOH and 99% CH_2Cl_2). Yield: 0.380 g, 40%. ^{1}H NMR ($CDCl_3$, 400 MHz): δ 8.13 (d, J = 8 Hz, 1H), 8.06 (s, 1H), 7.46 (d, J = 8 Hz, 1H), 7.41 (s, 1H), 7.0 (d, J = 8 Hz, 1H), 6.89 (d, J = 8 Hz, 1H), 6.16 (s, 1H), 6.02 (s, 1H), 4.02 (b, 2H), 3.54 (s, 3H), 3.03 (b, 2H), 1.98–1.93 (m, 2H), 1.84–1.78 (m, 8H), 1.42–1.38 (m, 2H), 1.24–1.06 (m, 52H), 0.89–0.81 (m, 9H), 0.74 (b, 2H), 0.48 (b, 2H); ^{13}C NMR ($CDCl_3$, 100.61 MHz): δ 181.8, 177.9, 172.1, 170.5, 169.7, 169.5, 147.3, 142.1, 141.9, 138.8, 131.3, 131.2, 130.8, 125.9, 125.6, 123.9, 117.5, 117.1, 110.9, 108.3, 88.3, 87.9, 59.3, 58.7, 48.4, 44.2, 40.3, 40.0, 31.9, 29.6, 29.5, 29.5, 29.3, 29.3, 27.2, 24.1, 22.1, 22.7, 22.6, 14.1; IR (cm^{-1}): 2954, 2920, 2853, 1701, 1598, 1565, 1490, 1464, 1425, 1350, 1266, 1216, 1085, 1056, 938, 809, 737, 709, 676, 658; MALDI-TOF (m/z): $[M]^+$ 981.663 $[M + H]^+$ and 983.736 $[M + H + 2]^+$.

2.3.4. (*E*)-4-((5-Carboxy-1,3,3-trimethyl-3*H*-indol-1-ium-2-yl)-methylene)-2-(((*Z*)-3-decyl-1,3-didodecyl-5-iodoindolin-2-ylidene)-methyl)-3-oxocyclobut-1-en-1-olate (ISQI). Starting materials **4d** (0.58 g, 0.79 mmol) and **5** (0.25 g, 0.79 mmol), reaction time 24 h, column chromatography (SiO_2, 100–200 mesh, from 1.5% MeOH and 98.5% CH_2Cl_2). Yield: 0.250 g, 30%. ^{1}H NMR ($CDCl_3$, 400 MHz): δ 8.11 (d, J = 8 Hz, 1H), 8.06 (s, 1H), 7.65 (d, J = 8 Hz, 1H), 7.58 (s, 1H), 7.01 (d, J = 8 Hz, 1H), 6.79 (d, J = 8 Hz, 1H), 6.16 (s, 1H), 6.02 (s, 1H), 4.01 (b, 2H), 3.54 (s, 3H), 3.02 (b, 2H), 1.97–1.91 (m, 2H), 1.84 (s, 8H), 1.42–1.39 (m, 2H), 1.24–1.06 (m, 52H), 0.87–0.82 (m, 8H), 0.73 (b, 2H), 0.47 (b, 2H); ^{13}C NMR ($CDCl_3$, 100.61 MHz): δ 182.1, 175.8, 170.3, 170.1, 168.1, 147.3, 143.6, 141.5, 130.9, 127.6, 123.7, 122.2, 109.6, 107.8, 88.2, 87.8, 59.1, 58.9, 49.3, 47.9, 44.0, 39.7, 31.7. 31.6, 29.4, 29.3, 29.2, 29.1, 29.0, 23.8, 22.4, 21.7, 17.4, 13.9; IR (cm^{-1}): 2957, 2921, 2852, 1701, 1596, 1568, 1487, 1465, 1422, 1350, 1267, 1214, 1088, 1056, 936, 795, 689, 654; MALDI-TOF (m/z): $[M]^+$ 1029.701.

2.4. General methods and instrumentation

General methods, experimental section, and characterization techniques are provided in the ESI.†

2.5. Dye-sensitized solar cell fabrication

DSSC fabrication and characterization for the **ISQ** dyes have been provided in the ESI.†[22]

3. Results and discussion

3.1. Synthesis of halogen-functionalized D–A–D-type unsymmetrical squaraine dyes

Synthesis of an unsymmetrical squaraine dye requires the condensation of a suitably functionalized indolium salt with the semisquaraic acid. The halo-substituted-4-hydrazinohydrochloride derivatives **1a–d** were reacted with branched ketone **2** to give the corresponding halo-substituted indolines **3a–d** *via* Fischer indole synthesis. The indoline derivatives **3a–d** were further reacted with 1-iododododecane to afford the corresponding branched-indolium salts **4a–d**. Condensation of indolium salts **4a–d** with the semisquaric acid **5** under the azeotropic removal of water afforded the required halogen-containing unsymmetrical squaraine dyes **6a–d** (Scheme 1) with moderate yields (30–40%). The final dyes were dark-blue solids and solubilized well in dichloromethane, chloroform, ethanol, and DMSO. All the newly synthesized compounds were characterized using ^{1}H-NMR, ^{13}C-NMR, and IR spectroscopic methods and mass spectrometry.

3.2. Photophysical and electrochemical properties

The UV-vis absorption and emission studies of the **ISQ** dyes, as well as the dye **SQS4**, were carried out in $CH_3CN/CHCl_3$ (95 : 5%) solutions at room temperature (Table 1). The solution UV-vis absorption spectrum for the indoline-donor-based squaraine dyes contain a sharp and intense peak ($\varepsilon > 10^5\ M^{-1}\ cm^{-1}$) at 640–646 nm due to the π–π* transition, and a vibronic side peak located at a higher energy of 580 nm appeared as the shoulder. Normalized absorption and emission spectra for the **ISQ** and **SQS4** dyes are displayed in Fig. 2a. A small red-shift was observed in the absorption band for the **ISQCl**, **ISQBr**, and **ISQI** dyes (λ_{max} 645 and 646 nm) compared to the **ISQF** and **SQS4** dyes (λ_{max} 641 and 642 nm). A similar phenomenon can be observed in the emission of the **ISQ** dyes (650–656 nm) compared to the **SQS4** dye (650 nm). The **ISQ** dyes showed molar extinction coefficients in the range of 2.1–3.1 × 10^5 M^{-1} cm^{-1}.

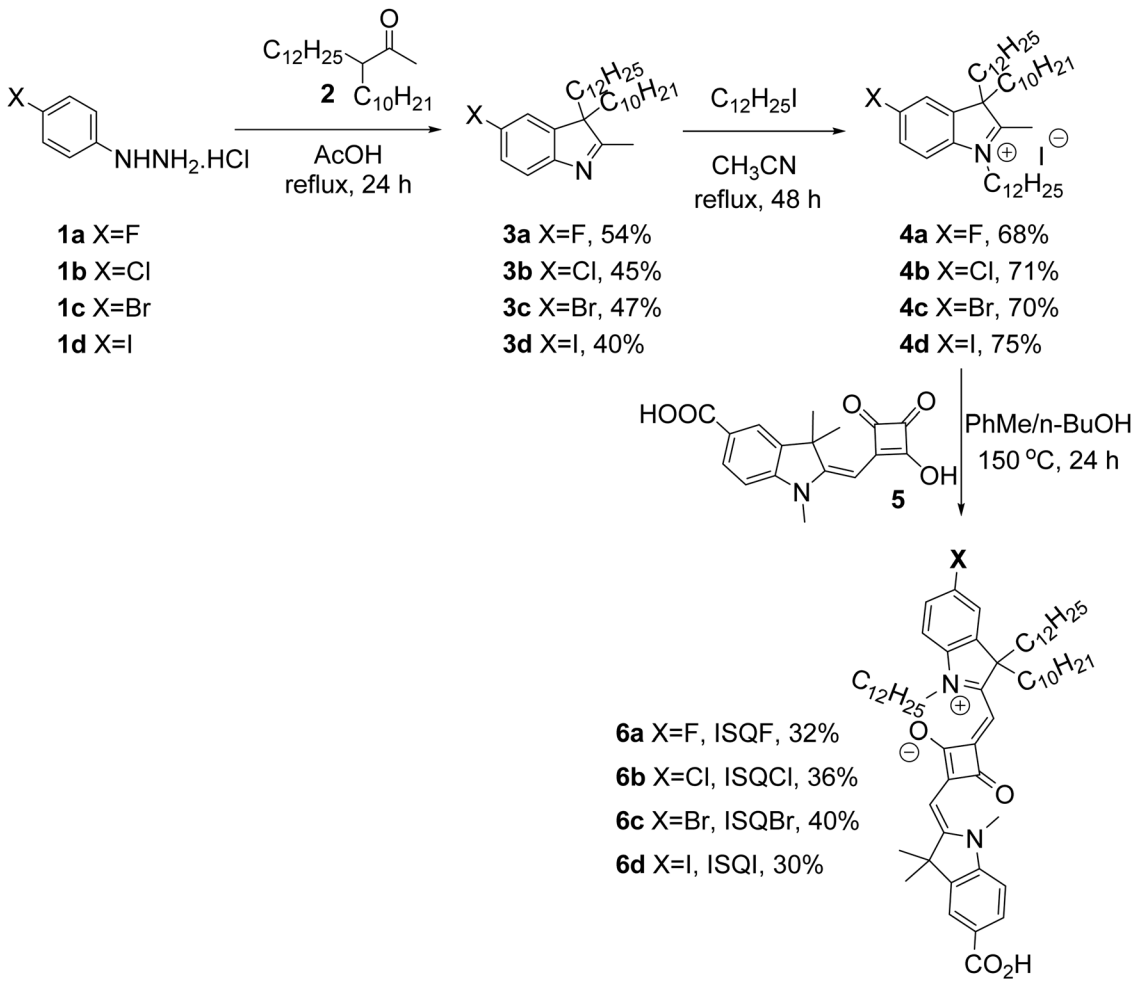

Scheme 1 Synthesis of halogen-containing (**ISQF**–**ISQI**) unsymmetrical squaraine dyes.

Table 1 Photophysical and electrochemical characterizations of **SQS4**, **ISQF**, **ISQCl**, **ISQBr** and **ISQI** dye at room temperature

Dye	λ_{max}[a] (nm)	λ_{max} TiO_2 (nm)	λ_{max}[b] (nm)	ε (10^5 M^{-1} cm^{-1})	LHE $\Delta\lambda$ at 60% (nm)	$E_{oxi.onset}$ (V *vs.* Ag/Ag^+)[c]	E_{ox} (V *vs.* NHE)[d]	E_{ox*} (V *vs.* NHE)	$E_{0\text{-}0}$[e] (eV)
ISQF	641	646	650	2.1	192	0.218	0.786	−1.12	1.91
ISQCl	645	656	654	2.5	209	0.260	0.828	−1.07	1.90
ISQBr	646	653	654	2.2	204	0.268	0.836	−1.06	1.90
ISQI	646	658	656	3.1	211	0.260	0.828	−1.07	1.90
SQS4	642	648	650	2.4	193	0.237	0.805	−1.10	1.91

[a] Absorption. [b] Emission of **ISQ** and **SQS4** in $CH_3CN/CHCl_3$ (95 : 5%) (excitation wavelength was 590 nm). [c] Oxidation potential. [d] E_{ox} reference electrode of $Ag/AgNO_3$ was used and was calibrated *vs* NHE *via* the addition of 0.7 V using ferrocene as an external standard. [e] $E_{0\text{-}0}$ optical band gap (from the intersect point of absorption and fluorescence, $1240/\lambda$).

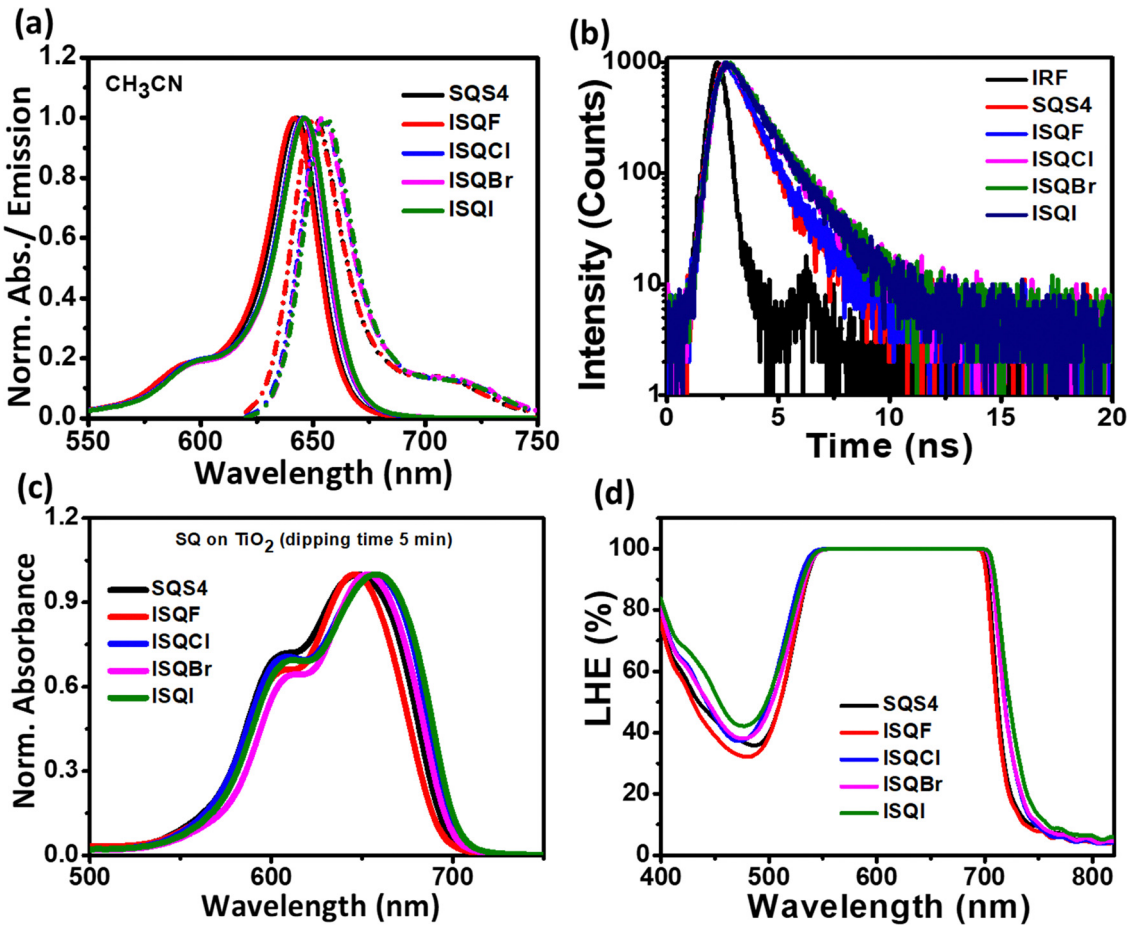

Fig. 2 (a) Normalized UV-vis and emission spectra of **SQS4**, **ISQF**, **ISQCl**, **ISQBr**, and **ISQI** in $CH_3CN/CHCl_3$ (95 : 5%) solution. (b) TCSPC decay profile for the **SQS4**, **ISQF**, **ISQCl**, **ISQBr**, and **ISQI** dyes in dichloromethane solution; excitation wavelength was 635 nm, emission monitored at 650 nm. (c) UV-vis absorption spectra of **SQS4**, **ISQF**, **ISQCl**, **ISQBr**, and **ISQI** dyes on the TiO_2 electrode. (d) LHE of **SQS4**, **ISQF**, **ISQCl**, **ISQBr**, and **ISQI** dyes on the TiO_2 electrode (LHE = $1\text{–}10^{-A}$).

Furthermore, to investigate the aggregation behaviour of the **ISQ** dyes on the metal-oxide surface and the light harvesting properties, UV-vis characterization was carried out on a TiO_2 surface. The dipping time of the electrodes was 5 min in a 0.1 mM dye solution prepared in MeCN: $CHCl_3$ (95 : 5) (Fig. 2c and Table 1). The **ISQ** and **SQS4** dyes all showed red-shifted charge transfer (π–π^*) peaks (646–658 nm), which correspond to the monomeric dye structure, with additional transition peaks for smaller aggregated structures between 605–610 nm compared to their solution spectra (643–649 nm) when the photoanode was sensitized for 5 min. In the presence of optically transparent co-adsorbent chenodeoxycholicacid (CDCA), competitive anchoring of CDCA on the metal-oxide surface reduces the dye–dye interaction, and hence, a reduction in the peak intensity at 605–610 nm was observed.(Fig. S10, ESI†). The light-harvesting efficiency (LHE) is one of the key factors in DSSCs; it represents

the ability of the sensitizers to absorb a certain range of photons for a particular dye. The LHE of the **ISQ** and **SQS4** dyes is displayed in Fig. 2d and Table 1 (sensitization time 12 h). The LHE properties of the **ISQF**, **ISQCl**, **ISQBr**, and **ISQI** dyes on the mesoporous TiO_2 thin films showed broad absorbance between 500–720 nm. The spectral broadening at 60% LHE increased from **SQS4** to **ISQI** ($\Delta\lambda$ = 193, 192, 209, 204, and 211 nm). This indicates that the extent of dye–dye interactions on the TiO_2 surface is almost the same for this set of dyes.

To investigate the photo-excited state properties of the **ISQ** dyes further, lifetime measurement using the time-correlated single-photon counting method (TCSPC) in dichloromethane (CH_2Cl_2) solutions was carried out (Fig. 2b, Table 2 and Table S1 in the ESI†). In general, the ground-state and the excited-state (S_0–S_1) electronic structures of D–A–D squaraine dyes are highly polarized, with the indoline moiety being an electron donor (D) and the central C_4O_2 unit being an electron acceptor (A). It is known that heavy-atom-functionalized organic chromophores undergo an efficient intersystem-crossing process to populate the triplet photo-excited state.[43,44] Thiosquaraine dyes are well-known chromophores for the triplet state; in these dyes, the oxygen atoms of C_4O_2 are replaced with sulfur atoms to form C_4S_2, and are responsible for the enhanced intersystem crossing (ISC).[45] Halogen atom incorporation outside the polymethine framework leads to enhanced fluorescence quantum yield, whereas, heavy atom functionalization within the polymethine framework leads to triplet-state formation.[46] **ISQ** dyes showed a biexponential lifetime with decay times τ_1 in the range of 0.79–1.10 ns. Furthermore, a relative method was used with the reference DMASQ dye (quantum yield 0.42 in dichloromethane solution) for the quantum yield calculations of the **ISQ** and **SQS4** dyes.[47] No significant changes were observed in the quantum yield (0.28 to 0.31%) for the **ISQ** and **SQS4** dyes. Hence, the charge injection takes place from the photoexcited singlet state of the **ISQ** dyes. As the heavy atoms are separated from the polymethine framework, spin–orbit coupling is not affected in these heavy-atom-containing **ISQ** dyes; hence, only the effect of halogen bonding is effectively considered for the dye regeneration.

Cyclic voltammetry studies were carried out in anhydrous dichloromethane solution to measure the electrochemical characteristics of the **ISQ** dyes (Fig. 3a and Table 1). The HOMO energy levels of the **ISQ** dyes were calculated from the first oxidation onset value of the cyclic voltammograms, which was converted to NHE by adding 0.7 V.[48] The ground state oxidation potential (E_{ox}) values of 0.79, 0.83, 0.84 and 0.83 V have been obtained for **ISQF**, **ISQCl**, **ISQBr**, and **ISQI** dyes *versus* NHE, respectively. The E_{ox} of the **ISQ** dyes was ~0.4 V more positive than the redox function of the I^-/I_3^- electrolyte (0.4 V *vs* NHE), which is favourable for the dye regeneration process. The excited state oxidation potential (E_{ox*}) energy levels were found by subtracting the optical band gap (E_{0-0}) from the E_{ox} values, which were found between −1.12 and −1.06 V and were favourable for the electron injection process for the **ISQ** dyes to the conduction band of TiO_2. The energy level diagrams of the **SQS4**, **ISQF**, **ISQCl**, **ISQBr**, and **ISQI** dyes with the DSSC device components are displayed in Fig. 3b.

Table 2 Fluorescence lifetimes of **ISQ** and **SQS4** dyes in CH_2Cl_2 at room temperature

Dye	τ_1 (ns)	a_1 (%)	τ_2 (ns)	a_2 (%)	χ^2	Quantum yield[a]
SQS4	0.79	86	0.17	14	1.24	0.28
ISQF	0.91	93	0.25	7	1.16	0.34
ISQCl	1.13	80	0.21	20	1.10	0.35
ISQBr	1.07	53	0.16	47	1.13	0.32
ISQI	1.10	76	0.19	24	1.08	0.31

[a] Using a relative method with DMASQ dye as a standard,[47] the absorbance values for **ISQ** dyes and the standard dye; DMASQ has been used as follows: **SQS4** (596 nm), **ISQF** (599 nm), **ISQCl** (593 nm), **ISQBr** (593 nm) and **ISQI** (590 nm).

3.3. Theoretical calculations

Using DFT calculations, the **ISQ** dye structures were optimized at the B3LYP/6-311G** and B3LYP/LANL2DZ (for **ISQBr** and **ISQI**) level using Gaussian 09;[49] the results showed that the inherent electronic structures, such as the HOMOs and LUMOs, were not affected by the presence of halogen atoms. The optimized structure for the **ISQI** dye and molecular electrostatic potential (MEP) mapped onto the van der Waals surface top view for the **SQ-X** and **ISQ-X**$^+$ dyes are provided in Fig. 4 and Fig. 5, respectively. The detailed optimized structures and corresponding tables are provided in the Supplementary information (Fig. S12–S18, and Tables S3–S5, ESI†). The HOMO of the **ISQ** dyes was mainly distributed over the polymethine framework, with lower electron densities at the indoline donors, and the LUMO was distributed over the carboxylic-acid-containing donor site in addition to the polymethine framework; this feature promotes the unidirectional charge injection process upon photoexcitation. Furthermore, the electrostatic potential plots of the dyes showed the presence of a σ-hole in the bromine- and iodine-containing **ISQ** dyes. Additionally, the DFT studies of the oxidised **ISQI** dye showed the contribution of the halogen atoms to the HOMO−1 level, as well as the presence of a σ-hole in the oxidized dye as indicated by the molecular electrostatic potential. These studies support the presence halogen atoms in **ISQBr** and **ISQI**, which may promote the dye-regeneration process by forming halogen bonding with the iodolyte electrolyte.

The interaction energies (ΔE) of the **ISQI** dye with the iodide ions of the electrolyte in its neutral (**ISQ-I**) and oxidised (**ISQ-I**$^+$) form were compared to that of the corresponding neutral and oxidised states of non-halogenated **SQS4** dye (**ISQ-H** and **ISQ-H**$^+$), respectively. The electrolyte interaction energy of the oxidised dye **ISQ-I**$^+$ was found to be lower than that of **ISQ-H**$^+$ by 10.71 kcal mol^{-1}. When the interaction distance between the **ISQ-I**$^+$ dye and I^- was investigated, it was found to show a 0.45 Å contraction, while **ISQ-H**$^+$ dye was found to show a 0.05 Å extension from the predicted van der Waals interaction distance (Fig. 6). Therefore, the calculations support the assumption that halogen bonding can exist between iodide and **ISQ-I**$^+$, and this effect is much more pronounced compared to its non-halogenated counterpart **ISQ-H**$^+$. Further analysis *via* a natural

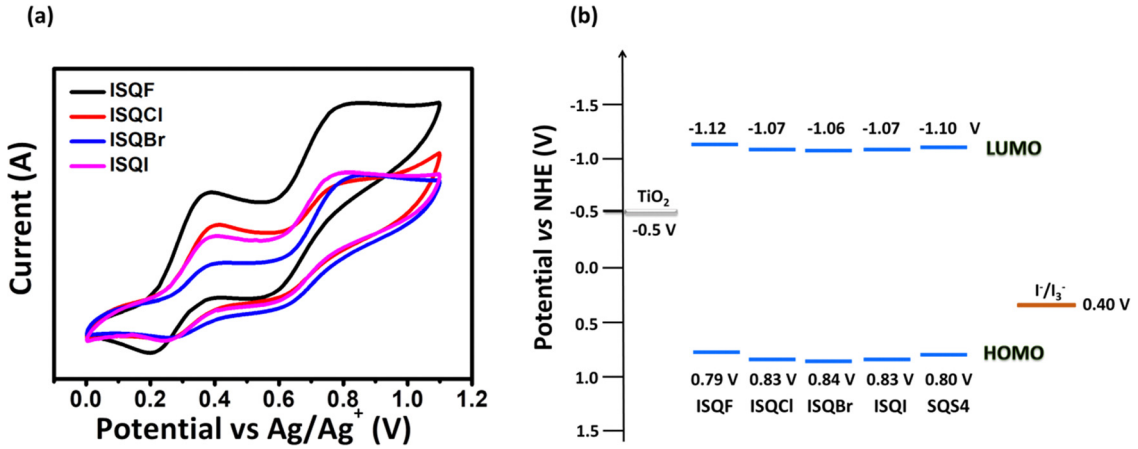

Fig. 3 (a) Cyclic voltammograms of the **ISQF**, **ISQCl**, **ISQBr**, and **ISQI** dyes. (b) Energy level diagram of the **ISQF**, **ISQCl**, **ISQBr**, and **ISQI** dyes along with the **SQS4** dye and DSSC device components.

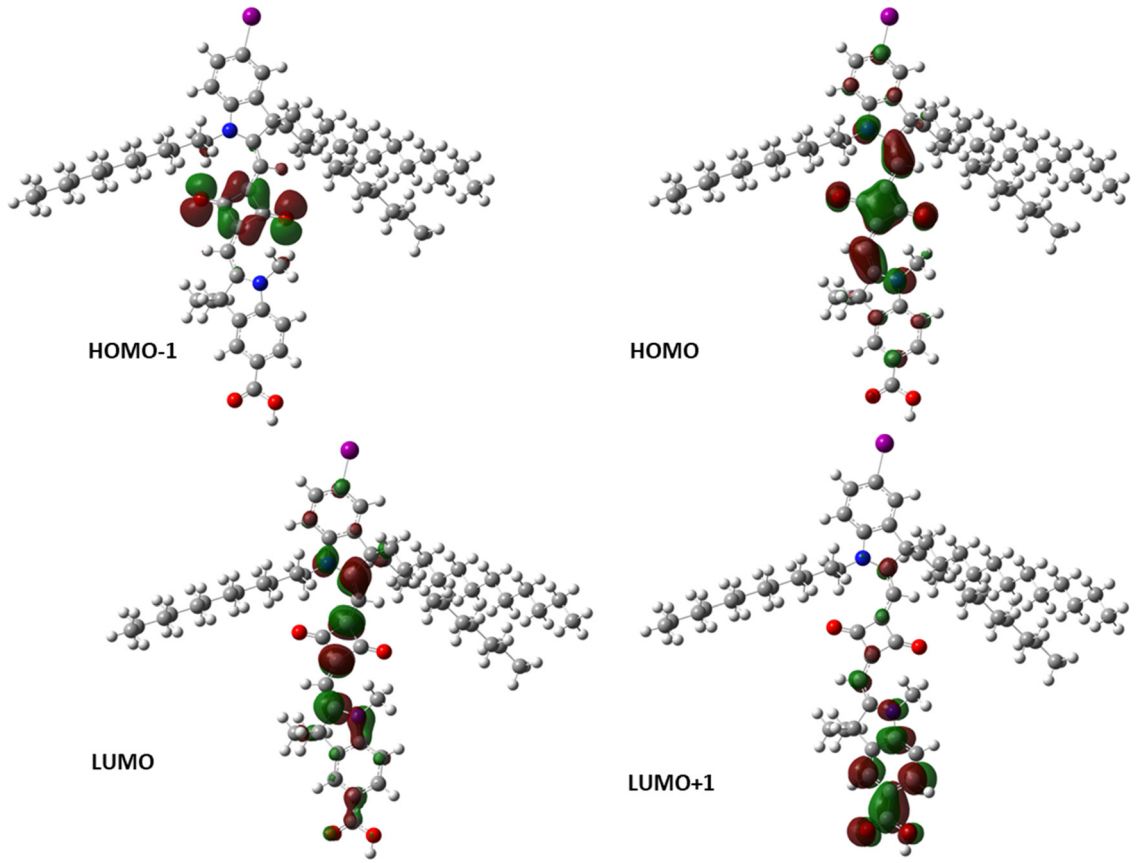

Fig. 4 DFT-optimized energy levels (HOMO, HOMO−1, LUMO, LUMO+1) of the **ISQI** dye.

bond orbital (NBO) study showed that the halogen bonding between the **ISQ-I** dyes and I^- corresponds to a Lewis acid–base adduct formed by a filled C–I σ bond to the empty π* orbitals of I^-. The orbitals associated with halogen bonding for the **ISQ-I**$^+$ and **ISQ-H**$^+$ dyes, along with the interaction stabilisation energy (E^2), are provided in Table 3. Interestingly, for neutral dyes, the **ISQ-H–I**$^-$ interaction is 6.06 kcal mol^{-1} lower than the **ISQ-I–I**$^-$ interaction, which is attributed to the 0.11 Å contraction in the van der Waals distance and an additional stabilisation between a lone pair on iodide and the empty C–X σ* orbital. The higher interaction energy of I^-, contraction from the predicted van der Waals distance and higher stabilisation energy support the observation that better halogen bonding is observed in the dyes with heavier halogen substituents. Hybridisation data for

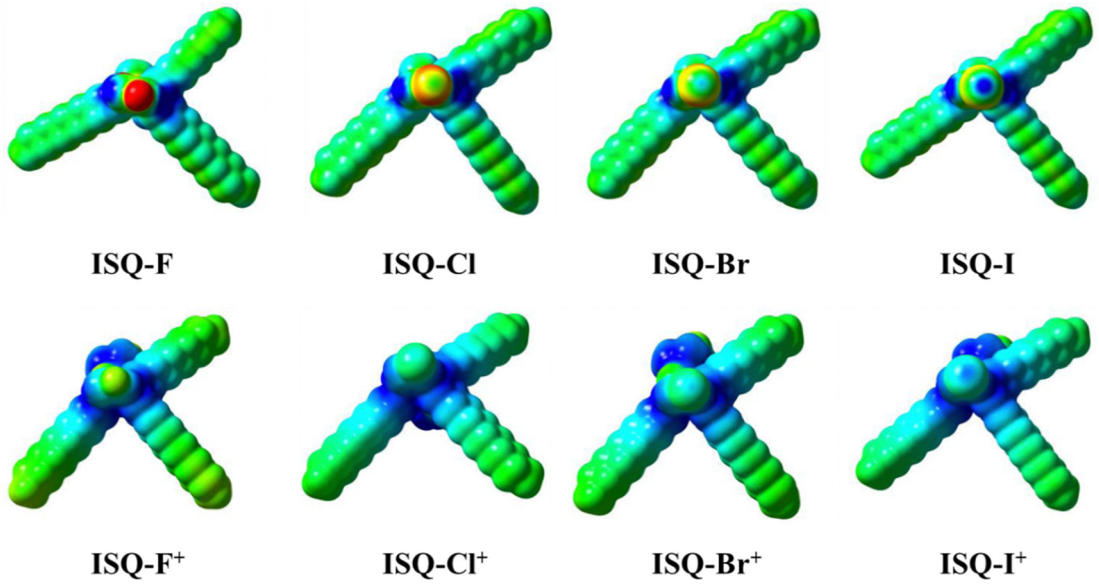

Fig. 5 Molecular electrostatic potential (MEP) mapped onto the van der Waals surfaces (top view) of the **ISQ-X** and **ISQ-X$^+$** dyes. The colour scale ( ) red to blue represents −0.02 to +0.02 kcal mol^{-1}.

selected orbitals for the donor–acceptor interaction with the I^- ion are provided in Table S8 (ESI†).

3.4. Photovoltaic characterization

Photovoltaic characterizations of the halogen containing **ISQ** dyes were carried out with two iodolyte electrolytes (I^-/I_3^-) and optimized using different concentrations of CDCA. As the IPCE is the product of light-harvesting efficiency (LHE), electron injection efficiency (φ_{inj}), charge collection efficiency (φ_{cc}), and dye regeneration efficiency (φ_{reg}) (eqn (1)),

$$\mathrm{IPCE}(\lambda) = \mathrm{LHE}(\lambda) \times \varphi_{inj} \times \varphi_{cc} \times \varphi_{reg} \quad (1)$$

The dye regeneration efficiency (φ_{reg}) depends on the concentration of the redox species as provided in the eqn (2) (where D = donor concentrations of (I^-), k_{reg} is the regeneration rate constant and k_{cr} is the charge recombination rate constant). The DSSC devices were fabricated with two different concentrations of iodolyte (concentration of I_3^- was 50 mM for Z-50 and 150 mM for Z-150).

$$\varphi_{reg} = \frac{k_{reg}[D]}{k_{cr} + k_{reg}[D]} \quad (2)$$

The photovoltaic parameters (V_{OC}, J_{SC}, ff, and η) are displayed in Fig. 7 and Table 4. The DSSC devices fabricated in iodolyte Z-50 without CDCA showed low J_{SC} values and DSSC efficiencies for the **ISQ** dyes compared to that for **SQS4** with a hydrogen atom. Use of iodolyte Z-150 as an electrolyte enhanced the J_{SC} and decreased the V_{OC} values for all the dyes in the absence of CDCA, and a maximum J_{SC} of 13.30 mA cm^{-2} was achieved using the **ISQI** dye.[9,50] The DSSC device fabricated with 3 equivalents of CDCA showed enhanced V_{OC}, J_{SC}, and efficiency for all the **ISQ** and **SQS4** dyes in both electrolytes (iodolyte Z-50 and Z-150) compared to the device sensitized in the absence of CDCA. **SQS4** dye in the absence of CDCA showed the maximum DSSC device efficiency compared to the **ISQ** dyes in both electrolyte systems (iodolyte Z-50 and Z-150). The **ISQI** dye with 3 equivalents of CDCA showed greater device efficiency compared to the other **ISQ** dyes and **SQS4** dye in both iodolyte Z-50 and Z-150 electrolytes. Furthermore, it was observed that the **ISQBr** dye sensitized with CDCA showed enhanced DSSC efficiency in iodolyte Z-150 electrolyte compared to the non-halogenated **SQS4** dye. The maximum DSSC device efficiency of 7.81% (with V_{OC} of 692 mV, J_{SC} of 15.06 mA cm^{-2}) was achieved using **ISQI** dye in iodolyte Z-150 electrolyte when the **ISQI** dye was sensitized with 3 equivalents of CDCA. The **ISQ** dyes showed excellent IPCE responses from the visible and NIR regions. The enhanced IPCE for the **ISQ** dyes in iodolyte Z-150 electrolyte was the reason for the improved J_{SC} compared to iodolyte Z-50 electrolyte. Additionally, a high-concentration electrolyte enhances the halogen bonding between the oxidized **ISQBr** and **ISQI** dyes on the TiO_2 and I^-; these interactions facilitate the dye-regeneration process, which in turn enhances the J_{SC} of the devices.[26,27] The low DSSC performance observed for **ISQF** and **ISQCl** compared to **SQS4** may be due to the electronic factors of the fluoride and chloride atoms on the indoline unit, respectively. A graphical representation of the V_{OC} and J_{SC} values in the iodolyte electrolytes (Z-50 and Z-150) for the **ISQ** and **SQS4** dyes in the presence and absence of CDCA is displayed in Fig. 8. The enhanced photocurrent generation with Z-150 compared to Z-50 indicates the interaction between the electrolyte and oxidized dye with halogen atoms compared to that for **SQS4**. The determination of dye regeneration rate constant would have provided more clear understanding. Furthermore, the amount of dye of adsorbed on the TiO_2 surface was calculated and provided in the Supplementary information (Fig. S20 and Table S7, ESI†).

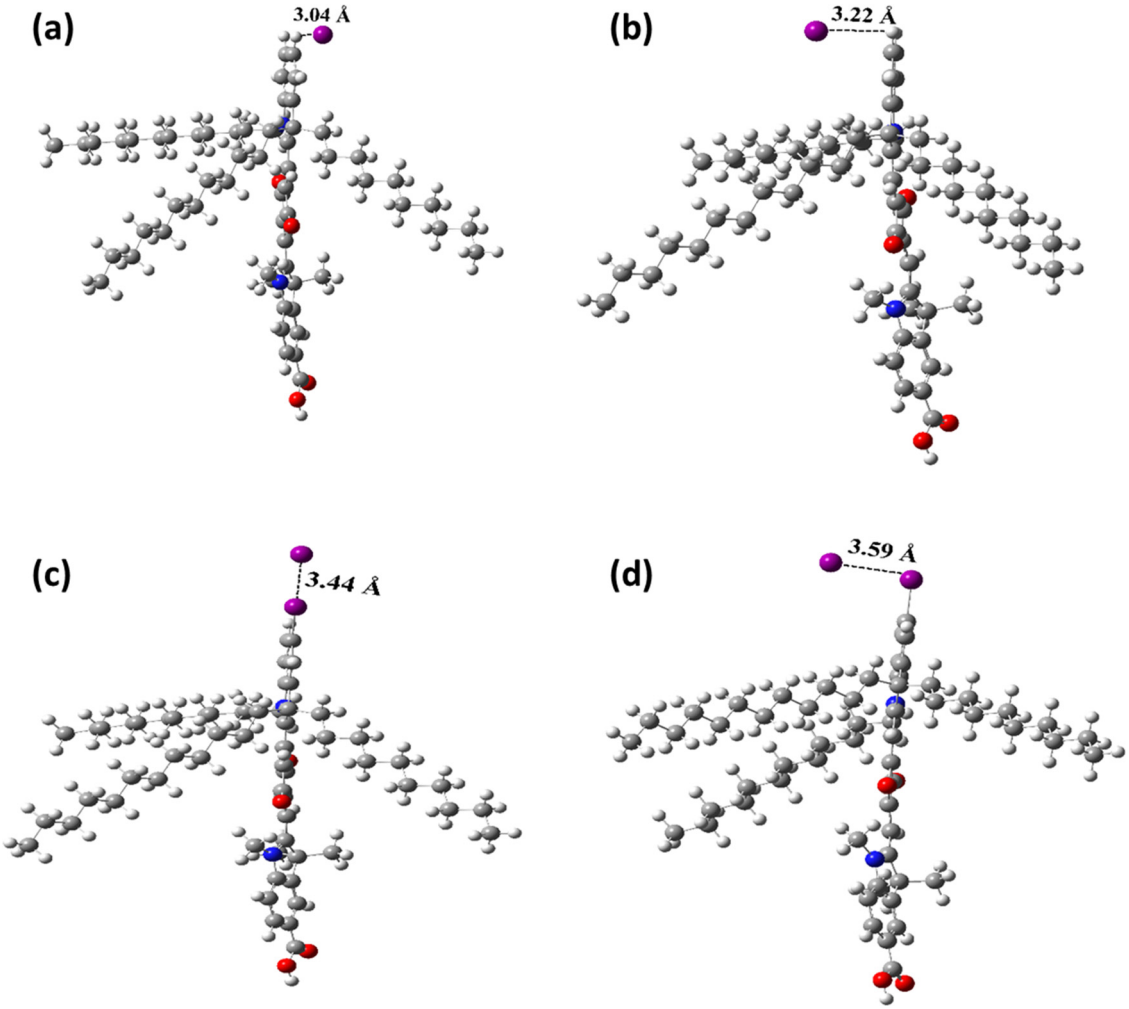

Fig. 6 Optimized structures of the **ISQ–I**$^-$ halogen–iodide interaction in (a) **ISQ-H**, (b) **ISQ-H**$^+$, (c) **ISQ-I** and (d) **ISQ-I**$^+$, with the dye–I$^-$ distances indicated.

Table 3 Calculated halogen–iodide distances, donor and acceptor with orbital contributions and stabilization energies (E^2) of the halogen–iodide interaction as shown in Fig. 6[a]

ISQ dye	ΔE (kJ mol^{-1})	Dye–I$^-$ (Å)	Donor	Acceptor	E^2 (kcal mol^{-1})
ISQ-H	−22.71	3.04	BD (1) C4–H152	RY*(1) I157	4.74
			LP (2) I 157	BD*(1) C4–H152	0.13
ISQ-I	−16.64	3.44	BD (1) C4–I156	RY*(2) I157	2.39
ISQ-H$^+$	−64.13	3.22	BD (1) C4–H152	RY*(1) I157	10.46
ISQ-I$^+$	−74.84	3.59	BD (1) C4–I156	RY*(1) I157	51.19

[a] van der Waals radii of I$^-$ (2.06 Å), H (1.09 Å) and I (1.98 Å); predicted van der Waals distance between ISQ-H–I$^-$ (3.15 Å) and ISQ-I–I$^-$ (4.04 Å). BD: Bonding orbital, LP: Lone-Pair orbital, and RY: Rydberg orbital; LP*, LP* and RY*: Virtual empty orbitals.

Photovoltaic characterizations of the **ISQI** dye with 0.3 mM of CDCA were carried out with different concentrations of I^-/I_3^- electrolytes to evaluate the effect of iodolyte concentration on the DSSC performance. The photovoltaic parameters are provided in Fig. 9 and Table 4. The DSSC device fabricated with a low-concentration electrolyte (0.25 M DMPII) showed a relatively low J_{SC} compared to those with the high-concentration electrolytes (0.50 and 0.75 M DMPII). The photovoltaic parameters for the different electrolyte concentrations are provided in the Supplementary information (Fig. S19 and Table S6, ESI†).

Current transient experiments for the **SQS4** and **ISQI** dyes were carried out by switching the light source on and off (for 20 s each) to investigate the effect of non-halogenated and halogenated squaraine dyes with different electrolyte concentrations on the regeneration efficiency of dyes (Fig. 10).[51] Both **SQS4** and **ISQI** dyes showed enhanced current with Z-150 iodolyte electrolyte compared to Z-50, which was further

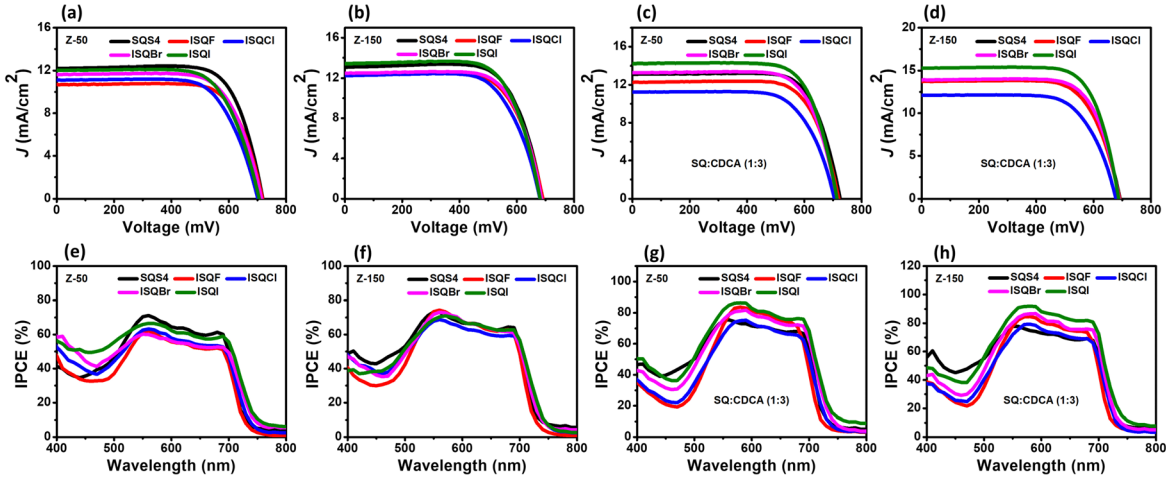

Fig. 7 *I–V* curves (a) and (c) in Z-50 and (b) and (d) in Z-150, and IPCE profiles in Z-50 (e) and (g) and in Z-150 (f) and (h) for the **ISQ** and **SQS4** dyes.

Table 4 Photovoltaic performance of **ISQ** dyes along with **SQS4** dye in Z-50 and Z-150[a]

Dye	CDCA (mM)	V_{OC} (mV) Z-50/Z-150	J_{SC} (mA cm^{-2}) Z-50/Z-150	*ff* (%) Z-50/Z-150	η (%) Z-50/Z-150
SQS4	0	719 ± 2.75/690 ± 1.46	12.18 ± 0.09/12.99 ± 0.08	74 ± 1.13/72 ± 0.96	6.48 ± 0.05/6.47 ± 0.12
ISQF	0	718 ± 1.77/691 ± 1.17	10.68 ± 0.07/12.2 ± 0.19	73 ± 1.24/71 ± 1.11	5.60 ± 0.06/5.99 ± 0.18
ISQCl	0	702 ± 2.56/681 ± 2.25	11.10 ± 0.04/12.20 ± 0.03	70 ± 0.81/70 ± 0.95	5.45 ± 0.10/5.82 ± 0.10
ISQBr	0	715 ± 1.53/687 ± 2.87	11.62 ± 0.18/12.44 ± 0.12	71 ± 1.15/71 ± 1.32	5.90 ± 0.18/6.10 ± 0.20
ISQI	0	705 ± 1.72/678 ± 3.90	12.01 ± 0.13/13.42 ± 0.15	70 ± 1.21/71 ± 1	5.92 ± 0.16/6.46 ± 0.25
SQS4	0.3	726 ± 1.73/693 ± 3.29	13.05 ± 0.19/13.65 ± 0.10	75 ± 0.83/72 ± 1.36	7.12 ± 0.19/6.85 ± 0.24
ISQF	0.3	721 ± 2.92/692 ± 1.09	12.20 ± 0.12/13.65 ± 0.10	73 ± 0.76/71 ± 0.82	6.44 ± 0.15/6.72 ± 0.16
ISQCl	0.3	705 ± 2.75/678 ± 2.47	11.18 ± 0.20/12.07 ± 0.05	70 ± 1.02/69 ± 1.00	5.53 ± 0.20/5.62 ± 0.14
ISQBr	0.3	715 ± 1.76/690 ± 1.28	13.21 ± 0.22/13.83 ± 0.15	74 ± 0.68/74 ± 0.94	6.99 ± 0.20/7.07 ± 0.28
ISQI	0.3	710 ± 3.14/690 ± 2.13	14.19 ± 0.07/15.28 ± 0.05	73 ± 1/74 ± 1.20	7.35 ± 0.10/7.80 ± 0.09
ISQI[b]	0.3	733 ± 1	10.61 ± 0.10	73 ± 0.88	5.67 ± 0.12
ISQI[c]	0.3	709 ± 2	12.21 ± 0.07	68 ± 0.50	5.81 ± 0.10

[a] Concentration of I_3^- was 50 mM or 150 mM. [b] Concentrations: 0.25 M DMPII, 15 mM I_2, 0.125 M NaI, 0.5 M TBP, 0.1 M GuSCN. [c] Concentrations: 0.50 M DMPII, 30 mM I_2, 0.250 M NaI, 0.5 M TBP, 0.1 M GuSCN. DMPII = 1,2-dimethyl-3-propylimidazolium iodide, TBP = 4-*tert*-butylpyridine, and GuSCN = guanidinium thiocyanate.

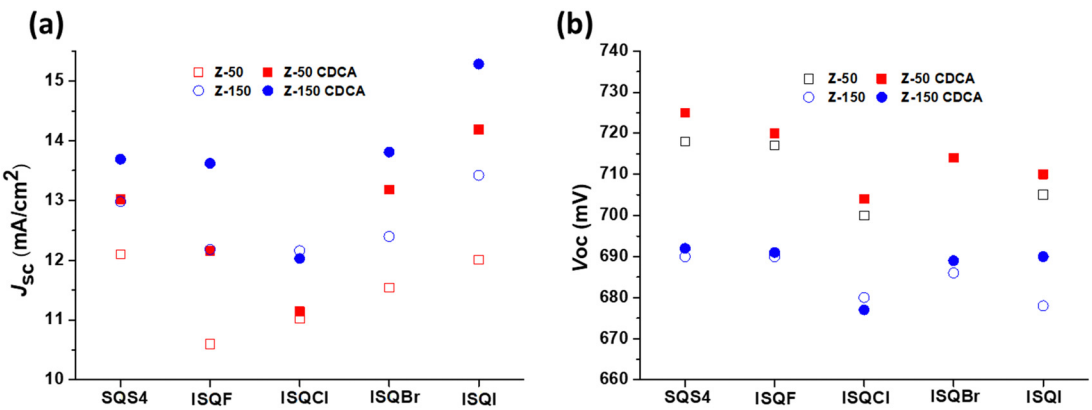

Fig. 8 Graphical representation of the (a) J_{SC} and (b) V_{OC} values of the halogen-containing **ISQ** dyes along with the **SQS4** dye in iodolyte electrolyte (Z-50 and Z-150).

improved in the presence of CDCA for both dyes. Here, the **ISQI** dye showed high current responses at different sun intensities with both Z-50 and Z-150 iodolyte electrolytes compared to **SQS4** dye, which clearly showed the importance of halogen-atom-containing squaraine dyes in achieving high DSSC J_{SC} and efficiency. A combined current transient profile of the **SQS4**

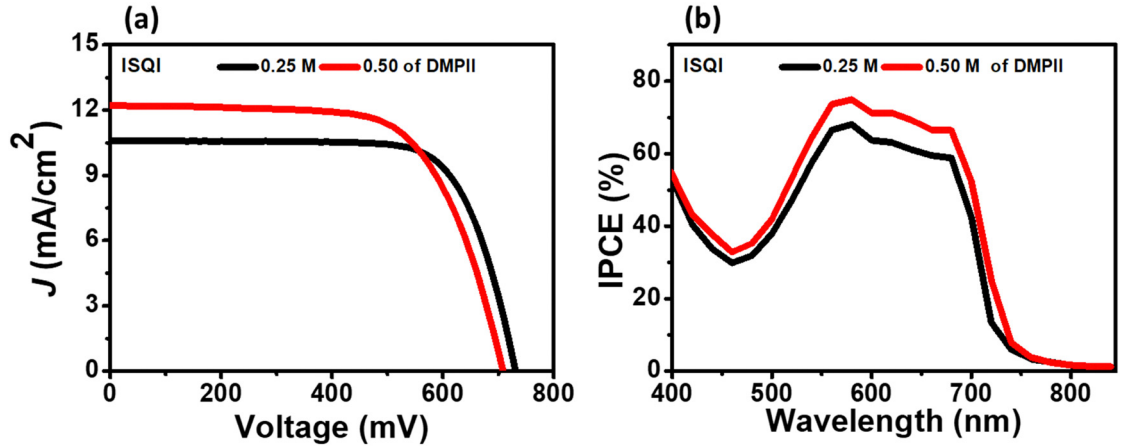

Fig. 9 (a) *I*–*V* and (b) IPCE curves of the **ISQI** dye with different concentration electrolytes.

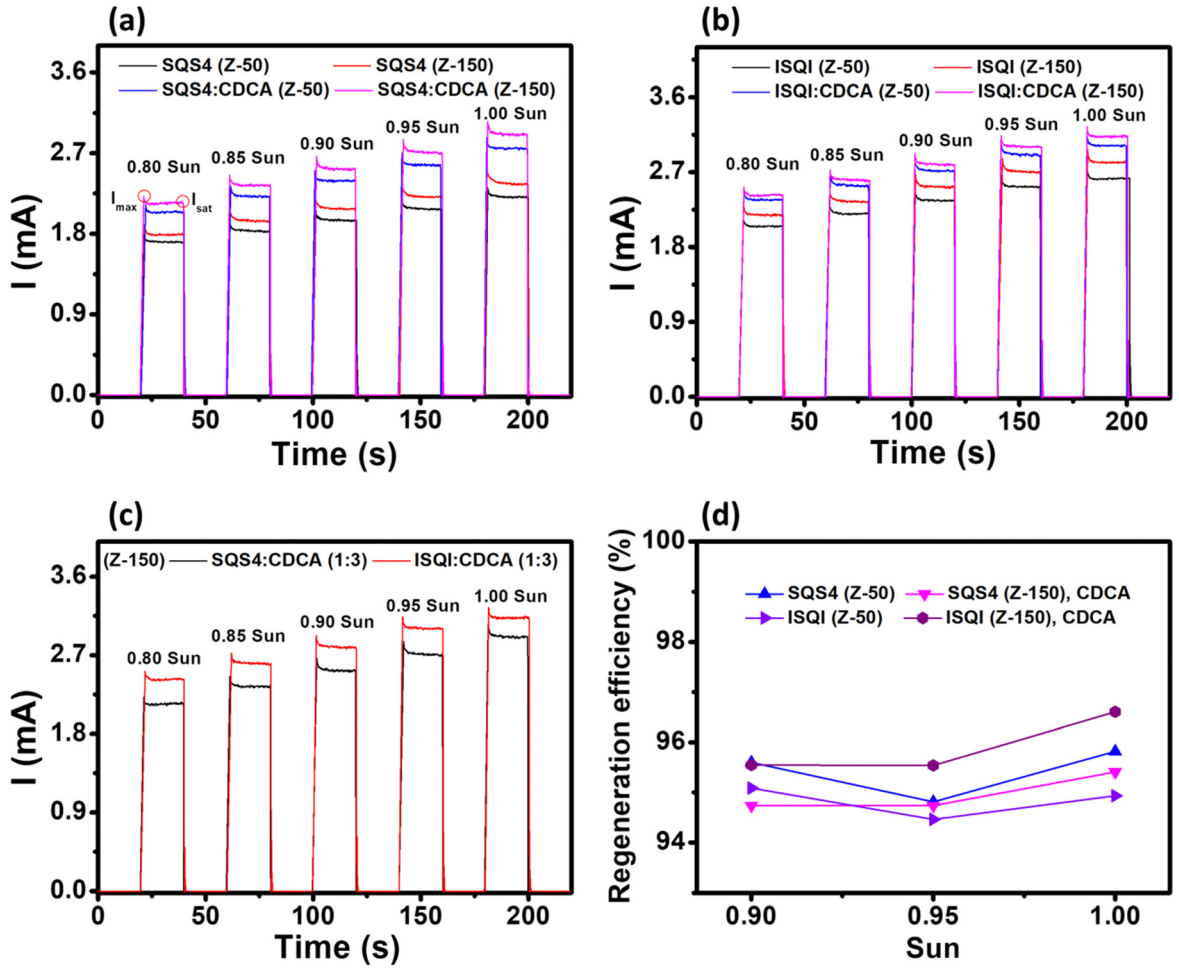

Fig. 10 Current transient profiles of (a) **SQS4** and (b) and **ISQI** in different CDCA electrolyte concentrations. (c) **SQS4** and **ISQI** with CDCA in Z-150 electrolyte. (d) Regeneration efficiency of **SQS4** and **ISQI** dyes with Z-50 and Z-150 iodolyte electrolyte in the presence of CDCA at different sun intensities.

and **ISQI** dyes with CDCA in Z-150 electrolyte is provided in Fig. 10c for better understanding. Furthermore, the regeneration efficiency (RE(%) = (I_{sat}/I_{max}) × 100) of the **SQS4** and **ISQI** dyes with CDCA at different sun intensities and electrolyte

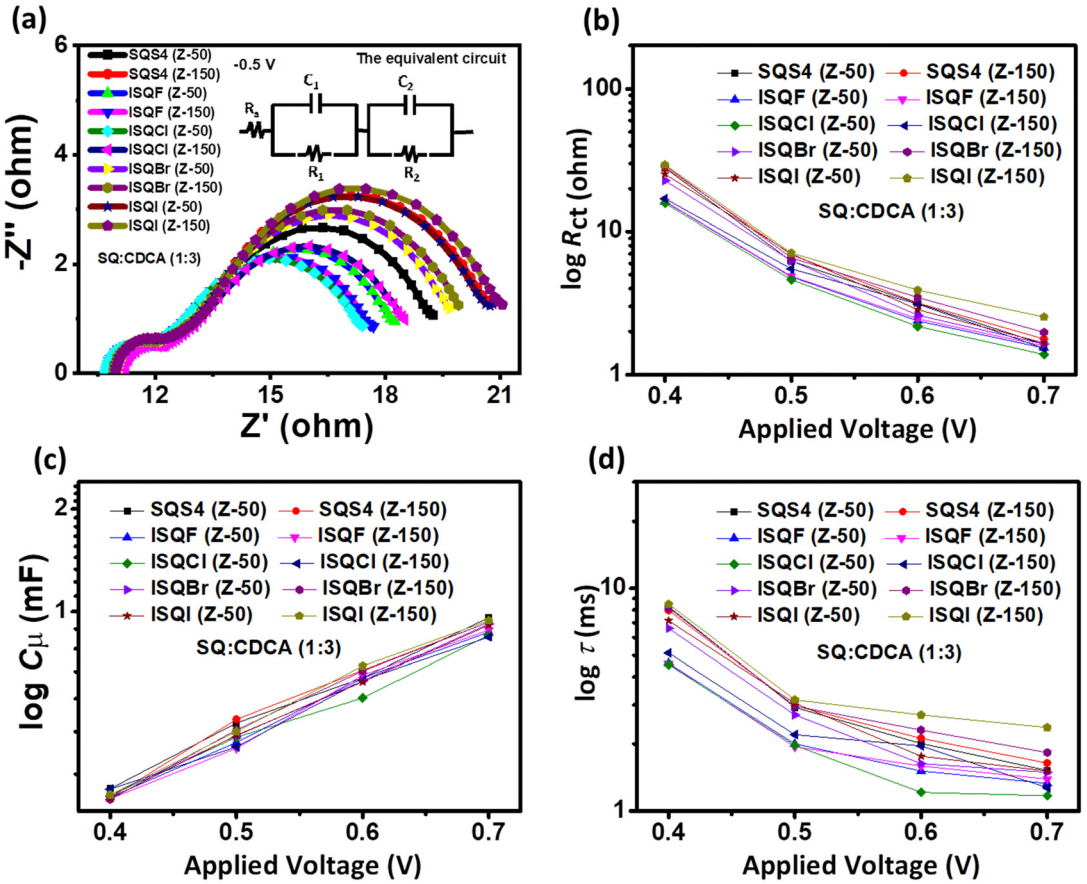

Fig. 11 (a) Nyquist plots, (b) R_{ct}, (c) C_{μ}, and (d) τ of the **ISQ** and **SQS4** dyes with iodolyte electrolyte (Z-50 and Z-150) in the presence of CDCA.

concentrations has been calculated (Fig. 10d), and **ISQI** showed the highest RE of 96.6% with Z-150 electrolyte compared to **SQS4** at 1.0 sun light intensity. This improved regeneration efficiency can be explained by the interaction between the electrolyte and the iodine atom of **ISQI**. Furthermore, the zwitterionic structures of the squaraine dyes might be the reason for the low RE compared to neutral D–π–A dye with iodolyte electrolytes at different light intensities.[51]

3.5. Electrochemical impedance spectroscopy (EIS)

To understand the charge recombination resistance (R_{ct}), chemical capacitance (C_{μ}), and lifetime of electron (τ) at the dye–TiO_2/electrolyte interface, EIS characterization of the halogen-containing **ISQ** dyes was carried out in the dark at different applied potentials with iodolyte electrolyte (Z-50 and Z-150).[52] The EIS parameters optimized with CDCA are provided in Fig. 11 and Table 5, and the EIS study without CDCA is provided in Fig. S21 (ESI†). As the **ISQ** and **SQS4** dyes have similar steric features, no significant changes are observed in the R_{ct}, C_{μ}, and τ when the electrolyte used for device fabrication was iodolyte Z-50 or Z-150 for all the dyes (Table 5) with CDCA. The maximum of values of 7.12 Ohm, 0.445 mF, and 3.16 ms for R_{ct}, C_{μ}, and τ were achieved for the **ISQI** dye with iodolyte Z-150 in the presence of CDCA, and are the reason for its high device efficiency compared to **SQS4** and the other **ISQ** dyes. It is observed that better R_{ct} parameters from the EIS

Table 5 EIS parameters of **ISQ** and **SQS4** dyes in the dark with iodolyte electrolyte (Z-50 and Z-150) and an applied bias of 0.50 V

Dye	R_{ct} (Ohm) Z-50/Z-150	C_{μ} (mF) Z-50/Z-150	τ (ms) Z-50/Z-150
SQS4	6.00 ± 0.09/6.03 ± 0.24	0.461/0.468	2.72/2.82
SQS4:CDCA (1 : 3)	6.23 ± 0.10/6.93 ± 0.08	0.471/0.483	2.92/2.97
ISQF	4.40 ± 0.28/4.43 ± 0.25	0.392/0.41	1.72/1.81
ISQF:CDCA (1 : 3)	4.85 ± 0.25/4.89 ± 0.18	0.413/0.40	2.00/1.94
ISQCl	4.65 ± 0.19/6.01 ± 0.22	0.432/0.437	2.00/2.62
ISQCl:CDCA (1 : 3)	4.62± 0.15/5.50 ± 0.10	0.428/0.401	2.62/2.20
ISQBr	6.12 ± 0.08/5.70 ± 0.12	0.392/0.391	2.39/2.22
ISQBr:CDCA (1 : 3)	6.27 ± 0.20/6.58 ± 0.10	0.432/0.450	2.70/2.96
ISQI	6.10 ± 0.10/6.23 ± 0.19	0.413/0.418	2.51/2.60
ISQI:CDCA (1 : 3)	7.03 ± 0.22/7.12 ± 0.18	0.434/0.445	3.05/3.16

studies were correlated with lower V_{OC} of the DSSC devices with the Z-150 electrolyte. The introduction of any new functional group in the dye backbone changes the inherent properties of the dyes, such as dipole moment, which may affect the conduction band position of TiO_2 and hence produce the variation in the obtained V_{OC} of the devices, despite the increased R_{ct} obtained from the EIS studies.

4. Conclusion

To achieve the advantages of halogen bonding in enhancing the J_{SC} and efficiency of DSSCs, a series of halogen-atom-functionalized D–A–D based unsymmetrical squaraine dyes, **ISQF**, **ISQCl**, **ISQBr** and **ISQI**, have been synthesized and characterized for DSSC applications. UV-vis absorption and emission studies showed slight red-shifts when the H-atom was replaced with a halo-atom in the **ISQ** dyes. Additionally, fluorescence lifetime and quantum yield measurements revealed biexponential lifetimes with a decay time τ_1 in the range of 0.79–1.10 ns, and the observed quantum yields of 0.28–0.31% did not show significant changes for the **ISQ** dyes. The DSSC devices for **ISQ** dyes were fabricated using iodolyte electrolytes (Z-50 and Z-150) and optimized with CDCA. The **ISQ** dyes showed varied photovoltaic characteristics with both electrolytes in the absence of CDCA. Sensitization of the **ISQ** dyes with 3 equivalents of CDCA showed enhanced photovoltaic parameters compared to those obtained without CDCA sensitization. The maximum DSSC device efficiency of 7.80% was achieved by the **ISQI** dye with a V_{OC} of 690 mV and J_{SC} of 15.28 mA cm^{-2} in iodolyte Z-150 electrolyte when the **ISQI** dye was sensitized with 3 equivalents of CDCA. The observed high DSSC device J_{SC} and efficiency in Z-150 electrolyte for the **ISQI** dye was due to the presence of a σ-hole, which enhanced the interaction between the electrolyte and the dye on TiO_2 and promoted the dye-regeneration process.

Author contributions

The manuscript was written through contributions of all authors. All authors have given approval to the final version of the manuscript.

Conflicts of interest

The authors declare no competing financial interest.

Acknowledgements

The financial support by SERB, India (CRG/2020/003105), and CSIR, India (NWP0054, CSIR-TAPSUN), are greatly acknowledged. I. S. N., A. K. S., A. M. and S. S. D. thank CSIR, New Delhi, India, for the research fellowships.

References

1 O. Regan and M. Grätzel, *Nature*, 1991, **353**, 737–740.
2 A. Hagfeldt, G. Boschloo, L. Sun, L. Kloo and H. Pettersson, *Chem. Rev.*, 2010, **110**, 6595–6663.
3 J. M. Ji, H. Zhou and H. K. Kim, *J. Mater. Chem. A*, 2018, **6**, 14518–14545.
4 A. B. Muñoz-García, I. Benesperi, G. Boschloo, J. J. Concepcion, J. H. Delcamp, E. A. Gibson, G. J. Meyer, M. Pavone, H. Pettersson, A. Hagfeldt and M. Freitag, *Chem. Soc. Rev.*, 2021, **50**, 12450–12550.
5 M. Ye, X. Wen, M. Wang, J. Iocozzia, N. Zhang, C. Lin and Z. Lin, *Mater. Today*, 2015, **18**, 155–162.
6 J. Wu, Z. Lan, J. Lin, M. Huang, Y. Huang, L. Fan and G. Luo, *Chem. Rev.*, 2015, **115**, 2136–2173.
7 A. Listorti, B. O'Regan and J. R. Durrant, *Chem. Mater.*, 2011, **23**, 3381–3399.
8 A. Y. Anderson, P. R. F. Barnes, J. R. Durrant and B. C. O'regan, *J. Phys. Chem. C*, 2011, **115**, 2439–2447.
9 S. Martiniani, A. Y. Anderson, C. H. Law, B. C. O'regan and C. Barolo, *Chem. Commun.*, 2012, **48**, 2406–2408.
10 Q. Yu, Y. Wang, Z. Yi, N. Zu, J. Zhang, M. Zhang and P. Wang, *ACS Nano*, 2010, **4**, 6032–6038.
11 J. Yang, F. Guo, J. Hua, X. Li, W. Wu, Y. Qu and H. Tian, *J. Mater. Chem.*, 2012, **22**, 24356.
12 Y. Wu, M. Marszalek, S. M. Zakeeruddin, Q. Zhang, H. Tian, M. Grätzel and W. Zhu, *Energy Environ. Sci.*, 2012, **5**, 8261.
13 Y. Jiao, F. Zhang, M. Grätzel and S. Meng, *Adv. Funct. Mater.*, 2013, **23**, 424–429.
14 J. Yang, P. Ganesan, J. Teuscher, T. Moehl, Y. J. Kim, C. Yi, P. Comte, K. Pei, T. W. Holcombe, M. K. Nazeeruddin, J. Hua, S. M. Zakeeruddin, H. Tian and M. Grätzel, *J. Am. Chem. Soc.*, 2014, **136**, 5722–5730.
15 N. Zhou, K. Prabakaran, B. Lee, S. H. Chang, B. Harutyunyan, P. Guo, M. R. Butler, A. Timalsina, M. J. Bedzyk, M. A. Ratner, S. Vegiraju, S. Yau, C. G. Wu, R. P. H. Chang, A. Facchetti, M. C. Chen and T. J. Marks, *J. Am. Chem. Soc.*, 2015, **137**, 4414–4423.
16 S. Alex, U. Santhosh and S. Das, *J. Photochem. Photobiol., A*, 2005, **172**, 63–71.
17 K. R. Mulhern, M. R. Detty and D. F. Watson, *J. Photochem. Photobiol., A*, 2013, **264**, 18–25.
18 G. De Miguel, M. Ziółek, M. Zitnan, J. A. Organero, S. S. Pandey, S. Hayase and A. Douhal, *J. Phys. Chem. C*, 2012, **116**, 9379–9389.
19 A. Otsuka, K. Funabiki, N. Sugiyama, T. Yoshida, H. Minoura and M. Matsui, *Chem. Lett.*, 2006, **35**, 666–667.
20 A. Alagumalai, M. F. Munavvar, P. Vellimalai, M. C. Sil and J. Nithyanandhan, *ACS Appl. Mater. Interfaces*, 2016, **8**, 35353–35367.
21 A. K. Singh, M. F. Mele Kavungathodi and J. Nithyanandhan, *ACS Appl. Mater. Interfaces*, 2020, **12**, 2555–2565.
22 A. K. Singh and J. Nithyanandhan, *ACS Appl. Energy Mater.*, 2021, **4**, 13932–13942.
23 T. Daeneke, A. J. Mozer, Y. Uemura, S. Makuta, M. Fekete, Y. Tachibana, N. Koumura, U. Bach and L. Spiccia, *J. Am. Chem. Soc.*, 2012, **134**, 16925–16928.

24 F. J. Malzner, S. Y. Brauchli, E. C. Constable, C. E. Housecroft and M. Neuburger, *RSC Adv.*, 2014, **4**, 48712–48723.
25 C. Curiac, L. A. Hunt, M. A. Sabuj, Q. Li, A. Baumann, H. Cheema, Y. Zhang, N. Rai, N. I. Hammer and J. H. Delcamp, *J. Phys. Chem. C*, 2021, **125**, 17647–17659.
26 S. J. C. Simon, F. G. L. Parlane, W. B. Swords, C. W. Kellett, C. Du, B. Lam, R. K. Dean, K. Hu, G. J. Meyer and C. P. Berlinguette, *J. Am. Chem. Soc.*, 2016, **138**, 10406–10409.
27 F. G. L. Parlane, C. Mustoe, C. W. Kellett, S. J. Simon, W. B. Swords, G. J. Meyer, P. Kennepohl and C. P. Berlinguette, *Nat. Commun.*, 2017, **8**, 1–7.
28 M. Ayaz, J. Khan Kasi, A. Khan Kasi, M. Bokhari and G. Boschloo, *ACS Appl. Energy Mater.*, 2022, **5**, 4240–4246.
29 L. Zhao, P. Wagner, J. E. Barnsley, T. M. Clarke, K. C. Gordon, S. Mori and A. J. Mozer, *Chem. Sci.*, 2016, **7**, 3506–3516.
30 G. Cavallo, P. Metrangolo, R. Milani, T. Pilati, A. Priimagi, G. Resnati and G. Terraneo, *Chem. Rev.*, 2016, **116**, 2478–2601.
31 C. W. Kellett, P. Kennepohl and C. P. Berlinguette, *Nat. Commun.*, 2020, **11**, 1–8.
32 W. B. Swords, S. J. C. Simon, F. G. L. Parlane, R. K. Dean, C. W. Kellett, K. Hu, G. J. Meyer and C. P. Berlinguette, *Angew. Chem., Int. Ed.*, 2016, **55**, 5956–5960.
33 D. Nugegoda, L. A. Hunt, A. Devdass, H. Cheema, R. C. Fortenberry, J. W. Jurss, N. I. Hammer and J. H. Delcamp, *ACS Appl. Energy Mater.*, 2022, **5**, 1516–1527.
34 J. M. Ji, H. J. Lee, H. Zhou, Y. K. Eom, C. H. Kim and H. K. Kim, *ACS Appl. Mater. Interfaces*, 2022, **14**, 52745–52757.
35 A. L. Raithel, W. E. Meador, T. Y. Kim, R. J. Staples, J. H. Delcamp and T. W. Hamann, *J. Am. Chem. Soc.*, 2023, **145**, 1367–1377.
36 S. Khopkar and G. Shankarling, *Dyes Pigm.*, 2019, **170**, 107645.
37 J. He, Y. J. Jo, X. Sun, W. Qiao, J. Ok and T. Kim, *Adv. Funct. Mater.*, 2009, **19**, 2720–2727.
38 J. H. Yum, P. Walter, S. Huber, D. Rentsch, T. Geiger, F. Nüesch, F. De Angelis, M. Grätzel and M. K. Nazeeruddin, *J. Am. Chem. Soc.*, 2007, **129**, 10320–10321.
39 T. Geiger, S. Kuster, J. H. Yum, S. J. Moon, M. K. Nazeeruddin, M. Grätzel and F. Nüesch, *Adv. Funct. Mater.*, 2009, **19**, 2720–2727.
40 F. M. Jradi, X. Kang, D. Oneil, G. Pajares, Y. A. Getmanenko, P. Szymanski, T. C. Parker, M. A. El-Sayed and S. R. Marder, *Chem. Mater.*, 2015, **27**, 2480–2487.
41 Y. Shi, R. B. M. Hill, J. H. Yum, A. Dualeh, S. Barlow, M. Grätzel, S. R. Marder and M. K. Nazeeruddin, *Angew. Chem., Int. Ed.*, 2011, **50**, 6619–6621.
42 A. K. Singh and J. Nithyanandhan, *ACS Appl. Energy Mater.*, 2022, **5**, 1858–1868.
43 W. Nau, *ChemPhysChem*, 2011, **12**, 2496–2497.
44 J. Zhao, W. Wu, J. Sun and S. Guo, *Chem. Soc. Rev.*, 2013, **42**, 5323.
45 D. Peceli, H. Hu, D. A. Fishman, S. Webster, O. V. Przhonska, V. V. Kurdyukov, Y. L. Slominsky, A. I. Tolmachev, A. D. Kachkovski, A. O. Gerasov, A. E. Masunov, D. J. Hagan and E. W. Van Stryland, *J. Phys. Chem. A*, 2013, **117**, 2333–2346.
46 S. Webster, D. Peceli, H. Hu, L. A. Padilha, O. V. Przhonska, A. E. Masunov, A. O. Gerasov, A. D. Kachkovski, Y. L. Slominsky, A. I. Tolmachev, V. V. Kurdyukov, O. O. Viniychuk, E. Barrasso, R. Lepkowicz, D. J. Hagan and E. W. Van Stryland, *J. Phys. Chem. Lett.*, 2010, **1**, 2354–2360.
47 C. Cornelissen-Gude, W. Rettig and R. Lapouyade, *J. Phys. Chem. A*, 1997, **101**, 9673–9677.
48 S. Aghazada, P. Gao, A. Yella, G. Marotta, T. Moehl, J. Teuscher, J. E. Moser, F. De Angelis, M. Grätzel and M. K. Nazeeruddin, *Inorg. Chem.*, 2016, **55**, 6653–6659.
49 M. J. Frisch; G. W. Trucks; H. B. Schlegel; G. E. Scuseria; M. A. Robb; J. R. Cheeseman; G. Scalmani; V. Barone; G. A. Petersson; H. Nakatsuji; X. Li; M. Caricato; A. Marenich; J. Bloino; B. G. Janesko; R. Gomperts; B. Mennucci; H. P. Hratchian; J. V. Ortiz; A. F. Izmaylov; J. L. Sonnenberg; D. Williams-Young; F. Ding; F. Lipparini; F. Egidi; J. Goings; B. Peng; A. Petrone; T. Henderson; D. Ranasinghe; V. G. Zakrzewski; J. Gao; N. Rega; G. Zheng; W. Liang; M. Hada; M. Ehara; K. Toyota; R. Fukuda; J. Hasegawa; M. Ishida; T. Nakajima; Y. Honda; O. Kitao; H. Nakai; T. Vreven; K. Throssell; J. A. Montgomery.; J. E. Peralta; F. Ogliaro; M. Bearpark; J. J. Heyd; E. Brothers; K. N. Kudin; V. N. Staroverov; T. Keith; R. Kobayashi; J. Normand; K. Raghavachari; A. Rendell; J. C. Burant; S. S. Iyengar; J. Tomasi; M. Cossi; J. M. Millam; M. Klene; C. Adamo; R. Cammi; J. W. Ochterski; R. L. Martin; K. Morokuma; O. Farkas; J. B. Foresman and D. J. Fox, *Gaussian 09*, Gaussian, Inc., Wallingford CT, 2016.
50 Z. Yu, M. Gorlov, J. Nissfolk, G. Boschloo and L. Kloo, *J. Phys. Chem. C*, 2010, **114**, 10612–10620.
51 S. C. Pradhan, A. Hagfeldt and S. Soman, *J. Mater. Chem. A*, 2018, **6**, 22204–22214.
52 Q. Wang, J.-E. Moser and M. Grätzel, *J. Phys. Chem. B*, 2005, **109**, 14945–14953.